 CMES, vol.3, no.5, pp.575-587, 2002

Computational Studies of Molecular Diffusion through Carbon Nanotube Based Membranes

Susan B. Sinnott[1], Zugang Mao,[2] and Ki-Ho Lee

Abstract: Nanofluidics is an area that has been under study for some time in zeolites and ideal nanoporous systems. Computational studies of the behavior of molecules in nanoporous structures have played an important role in understanding this phenomenon as experimental studies of molecular behavior in nanometer-scale pores are difficult to perform. In this paper computational work to study molecular motion and the separation of molecular mixtures in carbon nanotube systems is reported. The systems examined include organic molecules, such as CH_4, C_2H_6, n-C_4H_{10}, and i-C_4H_{10}, and inorganic molecules, such as CO_2. The interatomic forces in the molecular dynamics simulations are calculated using a classical reactive empirical bond-order hydrocarbon potential coupled to Lennard-Jones and Coulombic potentials. Molecules moving at thermal velocities corresponding to 300 K are predicted to diffuse from areas of high density to areas of low density through the nanotubes. The simulations indicate how the structure and size of the molecules and the nanotubes influence molecular diffusion through the nanotubes and the separation of the molecular mixtures.

1 Introduction

Carbon nanotubes have generated intense interest since their discovery in 1991 [Ijima (1991)] because of their unique mechanical, electrical and chemical properties . Their nanometer-scale size and hollow, cylindrical shape suggests that they may have many potential applications as molecular sieves, nano-test-tubes, and hydraulic actuators. Nanotubes might also be used in the production of tailored ultrafiltration membranes (membranes with pores on the order of 1-100 nm) [Caruana (1997); Cheryan (1986)]. Such a nanotube membrane might function by routing molecules through the channels between the close-packed tubes or through the middle of chemically opened [Dillon, et al. (1997); Sloan, et al. (1998); Liu, et al. (1998)] nanotubes.

It has been well established that diffusive flow is dominant in nanometer-scale ideal pores and zeolites [Karger, Ruthven (1992)]. Numerous computational studies have been undertaken to better understand and quantify diffusion in these nanometer-scale structures [Keffer, Davis, McCorick (1996); Keffer McCormick, Davis (1996); Sholl, Fichthorn (1997); Sastre, Catlow, Corma (1999); Mosell, Scrimpf, Brichmann (1997a); Mosell, Scrimpf, Brichmann (1997b); Gladden, Sousa-Goncalves, Alexander(1997); Webb, Grest, Mondello (1999), Saravanan, Auerbach (1999)]. Although carbon nanotubes share similarities with ideal pores and zeolites in that they contain nanometer-scale pores, this does not necessarily mean *a priori* that atomic and molecular diffusion in nanotubes will be the same as in ideal pores and zeolites. Several experiments have shown that numerous compounds and elements with low surface tensions intercalate into opened carbon nanotubes [Eswaramoorthy, Sen, Rao (1999); Ebbesen (1996)]. However, in these cases the nanotubes must have diameters large enough to accommodate capillary motion [Ugarte, Chatelain, de Heer (1996)]. These experiments confirm the predictions of early computational studies that showed that it is energetically favorable for small atoms or molecules to intercalate into small carbon nanotubes [Pederson, Broughton (1992); Breton, Gonzalez-Platas, Girardet (1994)].

Much attention has been focused on filling nanotubes with H_2 because using H_2 as an energy source is a topic of intense interest to a variety of sectors including energy and transportation. However, the study of H_2 storage in nanotubes has been controversial with contradictory experimental and theoretical results of uptake much

[1] Corresponding author
University of Florida
Deptarment of Materials Science and Engineering
Gainesville, Florida 32611-6400
sinnott@mse.ufl.edu
[2] Department of Materials Science and Engineering
Northwestern University, Evanston, Illinois 60208

higher than that of graphite and uptake about the same as that of graphite [Dillon, et al. (1997); Liu, et al. (1999); Ye, et. al (1999); Chen, Wu, Lin, Tan (1999); Yang (2000); Simonyan, Diep, Johnson (1999); Rzepka, Lamp, Casa-Lillo (1998); Wang Johnson (1999a); Wang, Johnson(1999b); Yin, Mays, McEnaney (2000); Lee, Lee (2000); Dresselhaus, Williams, Eklund (1999); Gordon, Saeger (1999); Darkrim, Levesque (1998); Darkrim, Levesque (2000); Brown, et al. (2000); Nutzenadel, et al. (1999)]. Noble gases, such as He, are predicted to condense in the interstitial sites within the pores to form an anisotropic phase with strong localization. Calculations predict that it is energetically more favorable for He atoms to reside in channels between close-packed carbon nanotubes rather than in a smooth, featureless pore of the same dimensions [Cole, et al. (2000)]. The binding energy of He in nanotube bundles has been measured at temperatures of 14 to 23 K and found to be quite large at around 0.02845 eV/atom for neutral surfaces at 330 K [Teizer, Hallock, Dujardin, Ebbesen (1999); Teizer, Hallock, Dujardin, Ebbesen (2000)]. It is assumed that the He atoms are in the channels between the nanotubes in the bundle.

Experiments find that when the carbon nanotube ends are opened chemically, the amount of Xe that can be adsorbed in the nanotubes increases dramatically [Kuznetsova, et al. (2000)]. The openings are initially blocked by carboxylic acid and quinone groups, so the opened nanotubes are heated to temperatures above 623 K to remove these groups and allow the Xe to enter the interior of the nanotube. The measured binding energies of 0.2778 ± 0.006 eV/atom agree with the theoretical estimates of 0.2343 eV/atom [Stan, Cole (1998)] for Xe adsorption in the interior of the nanotubes. The thermodynamic properties of monolayer films of hydrogen or noble gases adsorbed in tubes have also been calculated [Vidales, Crespi, Cole (1998)], and the structure of the films has been found to be strongly influenced by the structure of the nanotubes. Similar adsorption isotherms have been determined for CH_4 and Kr on single-walled nanotubes at low temperatures (78 - 110 K) and pressures (10^{-6} – 1 torr) [Muris, et al. (2000)] and are indicative of the formation of a single layer of gas on the outside of the tubes.

Adsorption isotherms of CH_4 on the outside of nanotube bundles where the nanotubes have closed ends have likewise been carried out at low temperatures between 150 and 200 K [Weber, et al. (2000)]. The binding energy is determined to be about 0.22 eV/molecule, which is about 76% higher than the adsorption energy on graphite. The increase is attributed to either the insertion of the CH_4 into the channels between the tubes or their adsorption to ridges on the exterior of the bundle. The condensation of CH_4 in nanotubes has been characterized by quasi-electron neutron scattering [Bienfait, Asmussen, Johnson, Zeppenfeld (2000)]. These measurements are used to determine the mobility of CH_4 in the nanotubes. In liquid-like CH_4, liquid and solid phases coexist. The fraction of liquid phase decreases as the temperature decreases from 50 to 91 K. When the temperature is below the melting point of 91 K, the mobility of the CH_4molecules decreases significantly as the amount of liquid phase disappears.

In this paper, we review and extend our previous computational work studying the diffusion of organic molecules (CH_4 and C_2H_6) and molecular mixtures (CH_4/C_2H_6, CH_4/n-C_4H_{10} and CH_4/i-C_4H_{10}) through carbon nanotubes and nanotube bundles, and report on preliminary new results for inorganic molecules such as CO_2. Some of these results have been published previously [Mao, Garg, Sinnott (1999); Mao, Sinnott (2000); Mao, Sinnott (2001)] and some new data is presented for the first time.

2 Computational Details

The computational approach used is classical molecular dynamics (MD) simulations, where Newton's equations of motion are numerically integrated to track the motion of the atoms with time [Allen, Tildesley (1987); Gear (1966); Gear (1971)]. A time step of 0.25 fs was used in all the simulations, which limits the results of the study to short time scales (ps to ns). The forces on the atoms are calculated using methods that vary with distance: short-range C–C and C-H interactions are calculated using a reactive empirical bonding order hydrocarbon potential that realistically describes covalent bonding within both the molecules and the carbon nanotubes. This potential was originally parameterized by Brenner to examine the growth of diamond thin films by chemical vapor deposition [Brenner (1990)] and has been widely used in many simulations of carbon nanotubes [Yakobson, Brabec, Bernholc (1996); Garg, Han, Sinnott (1998); Iijima, Brabec, Maiti, Bernholc (1996)]. The long-range C-C and C-H interactions are characterized

with Lennard-Jones (LJ) potentials [Ryckaert, Bellemans (1975)]. In the case of CO_2, the intramolecular bonds are held fixed and the atoms interact with each other and the nanotube walls via a combination of LJ [Murthy, O'Shea, McDonald (1983); Cui, Cochran, Cummings (1999)] and Coulombic [Brenner, et al (in press)] interaction potentials.

Thus, the combined expression used to calculate the energy of the system in each case is

$$U = \sum_i \sum_{i<j} [V_r(r_{ij}) - B_{ij} V_a(r_{ij}) + V_{vdw}(r_{ij}) + V_{Coul}(r_{ij})] \tag{1}$$

where U is the binding energy, r_{ij} is the distance between atoms i and j, V_r is a pair-additive term that models the interatomic core-core repulsive interactions, and V_a is a pair-additive term that models the attractive interactions due to the valence electrons. In addition, B_{ij} is a many-body empirical bond-order term that modulates valence electron densities and depends on atomic coordination and bond angles [Bremmer, et al. (in press)]. V_{vdw} is the contribution from the LJ potential and is only non-zero after the short–range covalent potential goes to zero. Thus, the first two terms describe covalent interactions only (except in the case of CO_2) while the LJ potential describes longer range intermolecular interactions and molecule-nanotube interactions. Figure 1 illustrates the C-C LJ interaction potential after the short-range, covalent potential has gone to zero. Finally, V_{Coul} is the Coulombic energy term which is only applicable to the CO_2 intermolecular interactions. The Coulombic energy terms have the following form:

$$V_{Coul}(r_{ij}) = \frac{1}{4\pi\varepsilon_0} \frac{q_i q_j}{r_{ij}} \tag{2}$$

where q_i and q_j are the partial charges on i and j (which equal 0.65 for C and –0.33 for O), r_{ij} is the interatomic distance, and ε_0 is the permittivity constant. The value of the Coulomb energy is thus:

$$V_{Coul}(\text{O}_2\text{C-CO}_2 \text{ interactions}) = +6.105/r_{CC}(\text{eV Å/Å}) \tag{3a}$$

$$V_{Coul}(\text{OCO-CO}_2 \text{ interactions}) = -3.053/r_{CO}(\text{eV Å/Å}) \tag{3b}$$

$$V_{Coul}(\text{OCO-OCO interactions}) = +1.526/r_{OO}(\text{eV Å/Å}) \tag{3c}$$

This form of the Coulomb potential was developed to describe supercritical CO_2 fluids [Cui, Cochran, Cummings (1999)] and is only applied to CO_2-CO_2 interactions (it is not applied to CO_2-nanotube interactions). No inramolecular potential terms are used to characterize the CO_2 molecules as their intramolecular geometry is frozen. However, they are able to rotate as they move through space. Figure 2 shows the combined potentials applied to the C and O atoms in the CO_2 molecules.

During equilibration 90% of the atoms in the system (molecules and nanotube wall atoms) have a Langevin thermostat [Allen, Tildesley (1987)] applied to them to quickly arrive at the ambient temperature of 300 K (except where noted). This is done to avoid computational artifacts that occur when 100% of the atoms have Langevin thermostats applied to them. All the atoms in the nanotube walls are allowed to move in response to applied forces according to Newton's equations and with the additional constraint of applied Langevin frictional forces. The nanotube axis varies in length between 80 Å and 150 Å and a range of nanotube diameters and helical structures are considered. The opened nanotubes are terminated with either C (in the form of truncated, open nanotubes with dangling bonds) or H atoms (that satisfy the truncated, open nanotubes). Both cases are considered to assess the effect of reactivity at the nanotube opening.

To set up the simulations the molecules of interest are placed near the opening at one end (some slightly inside the nanotube, some well outside the opening) and the system is allowed to evolve in time with no additional constraints. In some cases periodic boundary conditions are applied in the two directions normal to the nanotube axis in order to confine the molecules in a specified volume near the nanotube opening while leaving motion in the direction of the nanotube axis free. These starting conditions therefore correspond to an external molecular pressure gradient.

3 Results and Discussion

3.1 Organic Molecules

The simulations agree with previous studies in that they predict that the molecules intercalate into the nanotubes and diffuse down their length from areas of high density to areas of low density. However, the mechanisms followed vary with molecular size and shape and nanotube

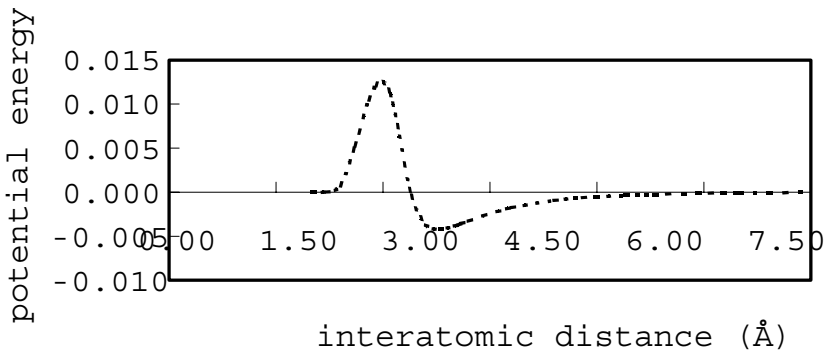

Figure 1 : Plot of the Lennard-Jones C-C interactions as a function of distance.

diameter. This is clearly shown in Tables I and II which summarize the results for the diffusion of pure gases of CH_4 and C_2H_6 in zigzag [62] nanotubes of various diameters. The results indicate that the CH_4 always follows normal-mode diffusion, which can be expressed as:

$$z^2 = 2At \tag{4}$$

where z is the average distance that the molecules travel in side the nanotube, A is the diffusion coefficient, and t is time. In this diffusion mode, individual molecules can pass each other within the nanotube. In contrast, C_2H_6 diffuses by single-file mode in the smallest diameter nanotubes, where individual molecules cannot pass each other because of their relatively large size and show the following relationship:

$$z^2 = 2Bt^{0.5} \tag{5}$$

where B is the diffusion mobility. As the nanotube diameter increases, these linear molecules switch to a mode that is intermediate between normal-mode and single-file diffusion. We have developed a general equation to quantify the description of this transition-mode diffusion as follows:

$$z^2 = 2Ct^n \tag{6}$$

where C is the diffusion mobility and n is a coefficient that depends on molecular type and pore diameter. The index n reflects the rate at which molecules can pass each other and provides an indication of the small-angle molecular rotation. As the nanotube diameter increases further, the diffusion mode of the C_2H_6 transforms to normal-mode diffusion.

These results indicate that if the molecular structure is spherical, as it is in CH_4, the diffusion behavior can be clearly distinguished as either normal-mode or single-file mode. However, if the molecular shape is highly asymmetrical, as is the case with C_2H_6, transition-mode diffusion can occur over the short time scales of this study. Transition mode diffusion occurs in nanotubes with diameters that are large enough for the molecules to pass each other if they are all perfectly aligned parallel to the nanotube axis, but not large enough to allow them to pass each other if some of them undergo small-angle rotational motion. For C_2H_6 this corresponds to nanotube diameters of about 0.8 – 1.4 nm.

It should be pointed out that combined Monte Carlo (MC) and MD simulations designed to study diffusion in zeolites over significantly longer time scales than those accessible here [Sholl (1999); Cuthbert, et al. (1999); Nelson, Scott (1999)] found that transition-mode molecular diffusion behavior resolved itself into normal-mode diffusion over time. In addition, MD studies [Hahn, Karger (1998)] show that when molecules have the ability to pass each other in the nanopore, small changes in the system can have a significant effect on the results, which further complicates the characterization of transition-mode diffusion. Temperature can to play a roll in determining the diffusion mode [Keffer (1999)], where slight increases in temperature allow molecules to squeeze past one another that might normally not be able to pass each other. Experimentally, no transition-mode diffusion has been observed, but different experiments show single-file and normal-mode diffusion for the same system [Cuthbert, et al. (1999)]. Thus, it should be recognized that Eq. 5 is primarily a way to quantify the motion of non-spherical molecules over short time scales as predicted in these simulations, rather than a universal expression.

Table I : Diffusion mode and coefficient for CH_4 in zigzag nanotubes of various diameters.

Nanotube	**Diameter(nm)**	**Diffusion mode**	**Diffusion Coefficient ($\times 10^{-4}$ cm^2/s)**
(9,0)	0.72	normal	3.91
(10,0)	0.80	normal	3.80
(12,0)	0.95	normal	2.94
(14,0)	1.11	normal	1.86
(16,0)	1.27	normal	1.05
(18,0)	1.43	normal	0.832
(20,0)	1.59	normal	0.425
(22,0)	1.75	normal	0.164

Table II : Diffusion mode and coefficients and mobilities for C_2H_6 in zigzag nanotubes of various diameters.

Nanotube	**Diameter(nm)**	**Diffusion mode**	**Diffusion Coefficient of Mobility**
(9,0)	0.72	single-file	$9.65\text{x}10^{-10}$cm^2/s$^{0.5}$
(10,0)	0.80	transition	$5.44\text{x}10^{-8}$ cm^2/s$^{0.74}$
(12,0)	0.95	transition	$8.15\text{x}10^{-7}$ cm^2/s$^{0.85}$
(14,0)	1.11	transition	$7.39\text{x}10^{-6}$ cm^2/s$^{0.92}$
(18,0)	1.43	normal	$9.65\text{x}10^{-5}$ cm^2/s
(20,0)	1.59	normal	$6.85\text{x}10^{-5}$ cm^2/s
(22,0)	1.75	normal	$2.92\text{x}10^{-5}$ cm^2/s

The effect of nanotube helical symmetry is examined by studying diffusion in similar diameter nanotubes that are either armchair or zigzag type. An example is the diffusion of CH_4 in (14,0) (radius = 0.556 nm) and (8,8) (radius = 0.550 nm) nanotubes under otherwise identical conditions. In both cases normal-mode diffusion is predicted. The diffusion coefficients are calculated to be $1.86\text{x}10^{-4}$ cm^2/s for the (14,0) nanotube and $1.78\text{x}10^{-4}$cm^2/s for the (8,8) nanotube. This indicates that the helical symmetry of the nanotube has little effect on the diffusion behavior of CH_4. However, this is not the case for C_2H_6 diffusion in nanotubes with diameters between 1.3 and 2.2 nm at low molecular densities. In these nanotubes, C_2H_6 molecules are predicted to follow a spiral path around the circumference of the nanotube so that the paths followed by the molecules are strongly correlated to the helical structure of the specific nanotubes. The driving force for this spiral diffusion path is that the interaction energy between C_2H_6 and the nanotube wall is maximized when the molecules line up with the C-C bonds in the nanotube wall. To maintain this high level of interaction energy, the molecules move forward by aligning with neighboring C-C bonds within the nanotube wall, which results in the helical path.

When C_2H_6 diffusion on graphite is considered, the simulations do not predict the lining up of the C-C bonds with the bonds in the graphite surface. In addition, the spiral diffusion path becomes more significant as the curvature of the nanotubes decreases. This indicates that the nanotube curvature serves to strengthen the interactions between the C_2H_6 and the C-C bonds in graphene. However, no spiral diffusion is predicted in nanotubes smaller than 1.3 nm where single-file or transition mode diffusion occurs. This is because when the nanotube diameter is very small, the linear C_2H_6 has too much difficulty lining up with the C-C bonds in the nanotube walls. In the case of nanotubes with diameters greater than 2.2 nm, the path of molecular motion becomes random destroying any tendency towards following a spiral path. This is also explained by the fact that as the curvature of nanotubes decreases, and the interaction between C_2H_6 and the nanotube walls decreases significantly.

When the initial density of C_2H_6 is varied from 0.408 to 0.156 g/cm^3, differences in diffusion behavior are predicted in the simulations. At low density almost all the molecules inside the nanotubes diffuse along a spiral path. At high density, the first three to eight molecules diffuse along the spiral path and the rest do not because the molecule-molecule interactions get stronger as the concentration of C_2H_6 in the nanotubes increases. Consequently, the C_2H_6-nanotube wall interactions are weakened and the C_2H_6 no longer follows a spiral route.

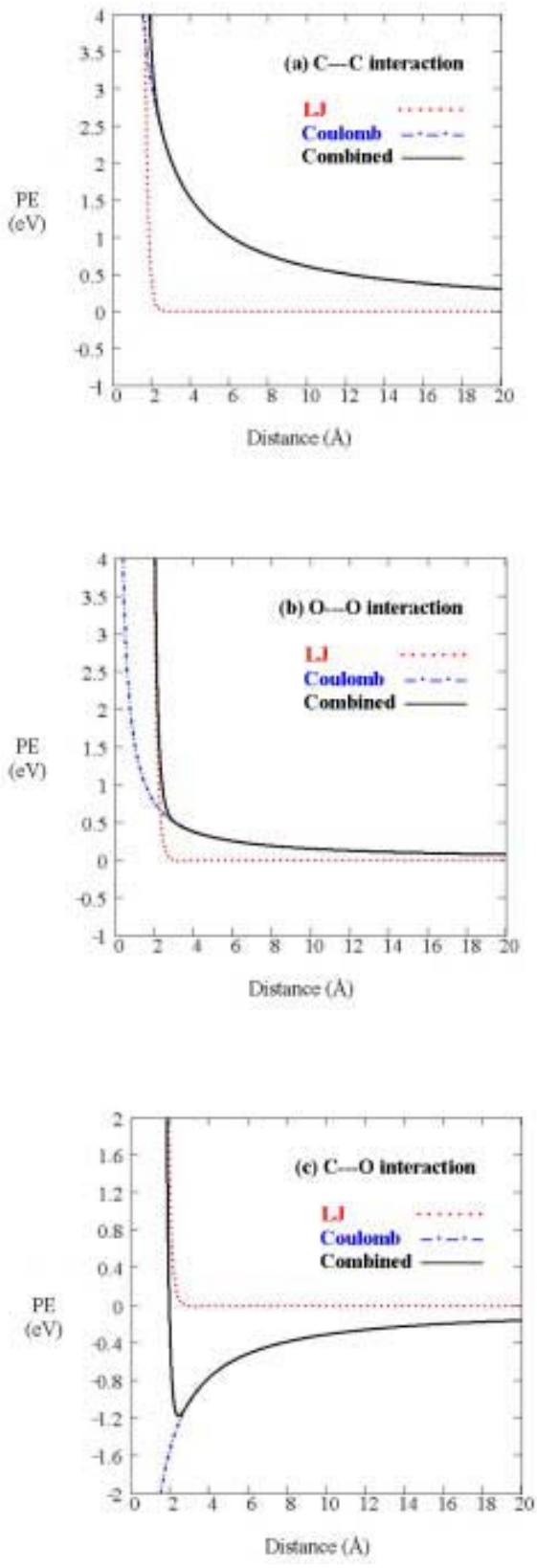

Figure 2 : Plots of the Lennard-Jones and Coulombic interactions (dotted lines) and their total (solid lines) for CO_2 for (a) C-C interactions, (b) C-O interactions and (c) O-O interactions.

This spiral diffusion path motion can ultimately be traced to the pairwise potentials used to calculated the interaction energy between the C_2H_6 and the nanotube. However, some experimental and first principles calculation evidence exists that similar behavior occurs for I_3^- and I_5^- intercalating in (10,10) tubes [Fan, et al. (2000)]. First principles calculations are currently underway to better understand this phenomenon.

When the nanotube diameters increase to 3.6 nm, in a (25,25) nanotube, no molecular diffusion is observed on the time scales of these classical MD simulations. It should be noted that 3.6 nm is the generally accepted cutoff for changes from diffusive motion to flow through other mechanisms, such as capillary motion [Morooka, Kusakabe (1999)]. Such motion could be investigated, for example, using a combination of MD and MC as done in [10].

The flux of CH_4 and C_2H_6 as a function of density in 0.8 nm (10,0) nanotubes is determined using the following expression:

$$J_j = -D_j(\partial C_j/\partial \quad z) \tag{7}$$

where the J_j is the flux or number of molecules that pass a given location per unit area, D_j is a constant, and $\partial C_j/\partial \quad z$ is the molecular density gradient along the tube axis. Figure 3 shows that the relation between the flux and the density gradient in nearly linear for CH_4 and C_2H_6. This suggests that the molecular motion is Fickian.

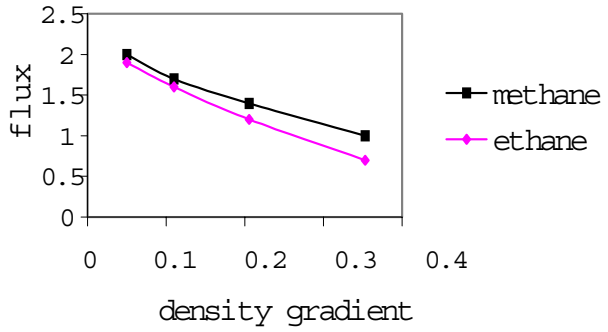

Figure 3 : Flux versus molecular density as calculated with Eq. (6) for CH_4 and C_2H_6 in (10,0) carbon nanotubes with diameters of 0.8 nm.

The effect of atomic termination at the nanotube opening is considered by comparing C-atom termination with H-atom termination. At low densities of CH_4, (0.110

g cm^{-3}), the molecules do not diffuse into H-atom terminated nanotubes as readily as into C-atom terminated nanotubes. However, as the density of CH_4 increases, the effect of atomic termination on the diffusion results decreases. For example, when the CH_4 density is 0.353 g cm^{-3} the diffusion coefficient for H-atom terminated nanotubes is about 2/3 of the value for diffusion into C-atom terminated nanotubes. In contrast, atomic termination has no significant effect on the diffusion of C_2H_6 at all the densities considered. This is because the smaller CH_4 molecules are more sensitive to the decreased attraction at the opening of the nanotube caused by H-atom termination while the large C_2H_6 molecules are not.

The effect of van der Waals correlations between neighboring nanotubes on the diffusion results are considered by examining the diffusive flow of CH_4 through a C-atom terminated (10,0) nanotube bundle, as illustrated in Figure 4, and a H-atom terminated (10,0) nanotube bundle (not shown). The diameters are 0.8 nm. The simulations show diffusion into the nanotubes but not into the interstitial sites between the nanotubes that are about 0.4 nm in diameter. This behavior can be explained by examining the interaction energy in these spaces: the energy of a CH_4 molecule inside one of the nanotubes is –0.24 eV/molecule while its energy in the interstitial site between the nanotubes is –0.16 eV/molecule. However, it is expected that the space between larger diameter nanotubes will become larger and interactions between them will decrease. These changes will make molecular intercalation into the channels more energetically favorable.

Compared to the diffusion in an individual (10,0) nanotube, the diffusion velocity through the bundle of nanotubes is slightly lower because the nanotube-nanotube (pore-pore) interactions decrease the molecule-nanotube-wall interactions. The constraint of the surrounding nanotubes in the bundle causes the nanotube walls to be fairly static during the diffusion process (although the atoms in the walls are free to move in the MD simulation). In contrast, in the case of the single-nanotube system, nanotube is very dynamic. Earlier studies by us [49] indicate that the more dynamic the nanotube, the more the motion of the atoms in the walls affects the diffusion process through collisions between the molecules and the nanotube walls that impart thermal energy from the nanotube to the molecules and vice versa. In the case of the bundle, the molecules do not collide as often with the nanotube walls and hence the kinetic energy of the molecules is used, and dissipated, through diffusion only. The calculated diffusion coefficient is 2.57x10^{-4} cm^2/s in the C-atom terminated case and 2.14x10^{-4} cm^2/s in the H-atom terminated case.

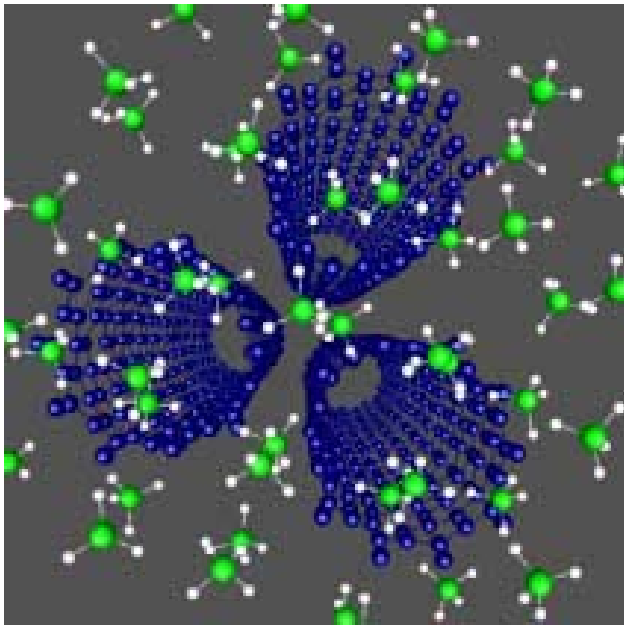

Figure 4 : Snapshot of CH_4 molecules diffusing through a bundle of (10,0) nanotubes.

3.2 Inorganic Molecules

Preliminary studies have been completed on the diffusion of CO_2 H-atom terminated (10,10) carbon nanotubes at 223 K. The results indicate that these molecules do not enter the nanotubes as readily as the organic molecules. Therefore, low molecular densities of CO_2 in the nanotube are seen in the simulations, as shown in Figure 5. Spiral diffusion is again predicted, with the C-O bond lining up with the C-C bonds in the nanotube walls. The reasons for this are similar to the reasons discussed above for the spiral diffusion of C_4H_6. Although the CO_2 molecules don't align in a special direction, they seem not to align along the vertical direction to the CNT length. It should be pointed out that the CO2 molecules are able to get closer to the nanotube walls and thus have interaction energies with the nanotube walls that are comparable to those of ethane and ethylene and significantly larger (by a few tenths of an eV) than the interactions of the spherical CH_4 with the nanotube walls. We are investigating the potential energies for various orientations of gas molecules, and for various distances be-

tween gas molecules and the wall of a CNT.

In behavior that is significantly different from the behavior of the organic molecules, the CO_2 molecules bounced did not leave the end of the nanotube but reversed their direction as they approached the open end. That makes it difficult to analyze the quantitative motion of the CO_2 in a manner similar to that done for the organic molecules. It is thought that this is related to the density of the gas in the CNT and can be removed by increasing the density of CO_2 at the mouth of the nanotube. This would increase the density gradient to continue to drive in CO_2 molecules and push them out the other end.

3.3 Molecular Mixtures

The specific molecular mixtures considered are CH_4/C_2H_6, CH_4/n-C_4H_{10}, and CH_4/i-C_4H_{10}. These molecules can be classified according to their linearity which has the following order:

$$\underset{spherical}{more} \; CH_4 = iso\text{-}C_4H_{10} < C_2H_6 < n-C_4H_{10} \; \underset{linear}{more}$$

In the analysis of the simulation results for molecular mixtures the flux, density profile, and diffusion coefficient/mobility of the molecules is determined in each system. For each molecular component, the flux of fluid, J, is determined by counting the net number of molecules that cross a given plane of certain area which is normal to the diffusion direction. The equation to calculate J is as follows[Bird, Stewart, Lightfoot (1976)]:

$$J = \frac{N - N'}{n\Delta t a} \tag{8}$$

where N is the number of molecules moving from the area of high density to the area of low density area, N' is the number of atoms moving from the area of low density to the area of high density, n is the number of simulation steps, Δt is the simulation time step, which is 0.25 fs in this study, and *a* is the area of the cross plane.

For multi-component systems, the diffusion patterns are complicated by the interactions among the different types of molecules. For this reason the Onsager theory of irreversible thermodynamic diffusion [Benes, Verweij (1999)] to describe the relation between the flux and the multi-diffusion coefficient. This theory is applicable to multi-component mixtures in microporous materials when the mechanical interactions between the different

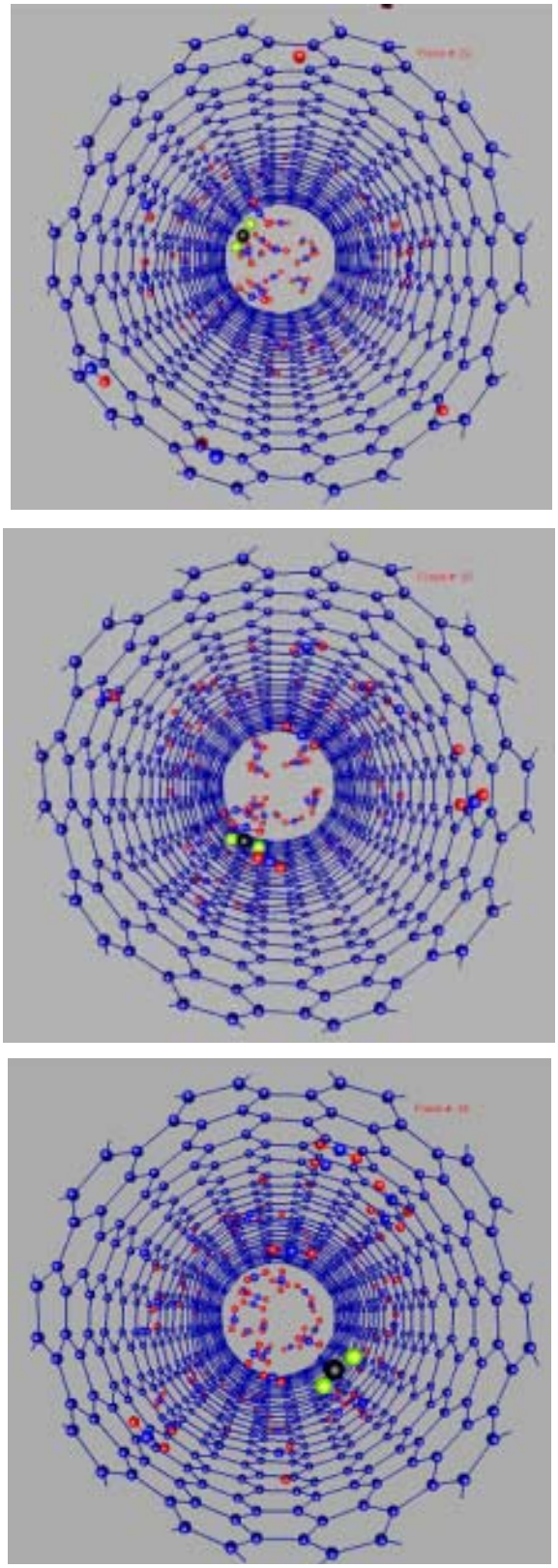

Figure 5 : Snapshots of CO_2 molecules diffusing through a single, H-atom terminated (10,10) nanotube taken at 11, 15, and 19 ps. A CO_2 molecule identified by a black colored carbon can be seen to follow a spiral path along the nanotube wall.

components can be neglected. The flux in this case is defined as:

$$J_i = -\frac{\rho q^{sat} D_i}{(1-\sum \theta j)}((1-\sum_{j\neq i}\theta_j)\frac{\partial \theta_i}{\partial z} + \theta_i \sum_{j\neq i}\frac{\partial \theta_j}{\partial z}) \quad (9)$$

The Onsager coefficient is defined as follows:

$$L_{ii} = \frac{\rho q^{sat} \theta_i Di}{RT} \quad (10)$$

where ρ is the molecular density, D_i is the mixed diffusion coefficient for component *i*, q^{sat} is the saturation volume of the molecules in the nanotubes and θ_i is the fraction of q^{sat} voids occupied by molecule i. This saturation state is calculated under the maximum loading of molecules in the nanotubes. The equation is solved under constant temperature and pressure conditions for the system under consideration. In our analysis of the simulation results we calculate the flux, J, using Eq. 7 directly from the simulations and check the quality of the results using Eq. 8. The mixed diffusion coefficient $D_i$here is similar to A of Eq. 3 but different from B and C of Eqs. 4 and 5. The Onsager theory is more complicated for cross-coefficients L_{ij} when there is significant mechanical interaction between the different components. These off diagonal Onsager coefficients can be computed from equilibrium MD simulations for arbitrary compositions without mechanical interactions [Sanborn, Snurr (2000)]. The separation coefficient, $T_{i/j}$, is used to analyze the separation trends in binary mixtures [MacElroy, Boyle (1999)]. We define the separation coefficient as follows:

$$T_{i/j} = \frac{\chi_j/\chi'_j}{\chi_i/\chi'_i} \quad (11)$$

here χ_i and $\chi_j$are the mole numbers of components i and j per unit volume at the end of nanotube, respectively, and χ'_iandχ_j' are the initial mole numbers of components i and j, respectively.

The results of the simulations and analysis are summarized in Table III. For a given binary mixture, as the diameters of the nanotubes decrease, the amount of separation of the molecular species increases. In addition, as the difference in the relative sizes of the molecules increases, the amount of separation of the molecular species also increases. In all cases, the molecular mixtures are characterized by large separation coefficients except for the CH_4/C_2H_6 system.

Both diffusion and adsorption are possible in the nanotubes for the larger n-C_4H_{10} and iso-C_4H_{10} molecules. For the very smallest nanotube diameters considered (0.7-1.1 nm) neither n-C_4H_{10} nor iso-C_4H_{10} go inside the nanotubes because they are too large while the CH_4 diffuses through the nanotubes by normal-mode diffusion. In this case the diffusion coefficient for CH_4 is almost the same as for the single component cases considered. In the medium diameter nanotubes (1.1-1.5 nm), both n-C_4H_{10} and iso-C_4H_{10} enter the nanotubes but stay in the middle of the pore because there is not enough room for them to get close to the walls due to the relatively high curvature of the nanotube and their relatively large sizes. Therefore, they diffuse down the center of the pore in single-file mode. In the largest diameter nanotubes considered (1.5-2.3 nm), both n-C_4H_{10} and iso-C_4H_{10} enter the nanotubes and have enough room to get close to the walls and adsorb. This behavior should be distinguished from the spiral diffusion behavior discussed above for C_2H_6 and CO_2. In this case absorption is characterized by the molecule staying in place. It is possible that over larger time scales than those accessible in the classical MD simulations the C_4H_{10} molecules would be transported by surface diffusion. The n-C_4H_{10} adsorbs more strongly than iso-C_4H_{10} because its larger linearity allows the bonds in the molecule to align with the carbon-carbon bonds in the nanotube. Neither CH_4 nor iso-C_4H_{10} can get as close to the nanotube walls because of their smaller degree of linearity. This is illustrated in Figure 6 which shows the flux of a CH_4/n-C_4H_{10} mixture in two different nanotubes across the nanotube diameter. The CH_4 stays near the middle of the nanotube while the n-C_4H_{10} stays near the nanotube walls. When n-C_4H_{10} and iso-C_4H_{10} adsorb to the walls, they partially block the pore and make it more difficult for CH_4 to go through, in agreement with the findings of [Gergidis, Theodorou, Jobic (2000)].

Thus, in all three cases separation of the C_4H_{10}/CH_4 mixture occurs. However, the mechanisms are fundamentally different. These simulation results agree with the available experimental data that shows that n-C_4H_{10} absorbs to the walls of multi-walled nanotubes with diameters of about 30 nm [Hilding, et al. (2001)].

The equilibrium adsorption energies of individual molecules on interior nanotube walls are considered separately to determine how they compare to one another and how they change with nanotube diameter. As the

Table III : Summary of the separation coefficients predicted for organic molecular mixtures in the indicated C-atom terminated nanotubes.

	(10,0)	(8,8)	(10,10)	(12,12)
CH_4/n-C_4H_{10}	Only CH_4diffuses	16.2	10.6	8.8
CH_4/i-C_4H_{10}	Only CH_4diffuses	25.5	14.3	7.9
CH_4/C_2H_6	2	1.5	1.1	

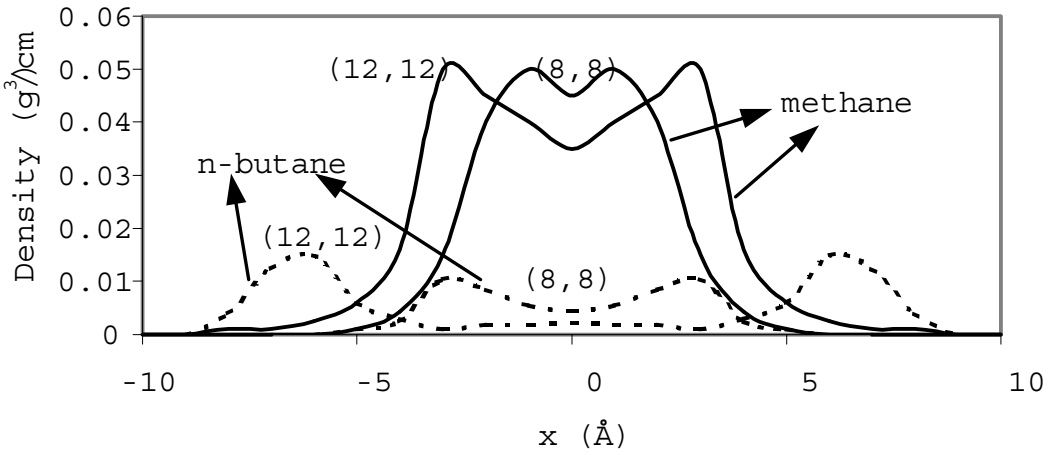

Figure 6 : The average density profile of the nanotubes in (8,8) and (12,12) nanotubes after 150 ps at 300 K for a CH_4/n-C_4H_{10} mixture.

nanotube diameter increases from about 0.8 nm to about 1.6 nm, the adsorption energy decreases for CH_4 (from about 0.3 eV/molecule to about 0.1 eV/molecule), C_2H_6 (from about 0.6 eV/molecule to about 0.4 eV/molecule) and iso-C_4H_{10} (from about 0.8 eV/molecule to about 0.6 eV/molecule). However, in the case of n-C_4H_{10} there is a slight increase (from about 1 eV/molecule to about 1.1 eV/molecule) with nanotube diameter. This is because the linear structure of the n-C_4H_{10} that allows it to line up to an optimum position close to the nanotube wall. The n-C_4H_{10} is able to get closer to the nanotube wall when the nanotube has less curvature. In addition, the larger molecules have higher adsorption energies than the smaller molecules.

Similar classical MD simulations have examined the motion of linear decanes inside SWNTs. The results indicate that a single layer forms on the wall at most densities [Zhang (1999)]. While the structures are anisotropic they show strong dependence on position relative to each other and to the nanotube walls. Most of the diffusion takes place in the center of the nanotube where the molecules are not "trapped" by the wall. In the case of molecular mixtures of gases, molecules with larger radii are able to adsorb to the walls more easily than smaller diameter molecules because they able to get closer to the wall [Ayappa (1998)].

Thus there are two factors that seem to most affect the diffusion behavior of molecules: one is the interaction between the molecules and the nanotube walls and the other is the interaction among the molecules themselves. The main driving force for diffusion is the first type of interaction listed. However, intermolecular interactions can have profound effects on the diffusion mechanism followed by a certain type of molecule. This is especially apparent in binary molecular mixtures where different types of molecules have different effects on each other during diffusion. This effect will increase as the size difference between different molecules increases. For CH_4/C_2H_6 mixtures, the behavior of both molecules is similar to their behavior in single-component systems. However, there are more significant differences in the behavior of CH_4 in CH_4/C_4H_{10} systems.

The conditions in these simulations are those of non-equilibrium MD since the molecular density of the first molecules to enter the nanotube differs from the density of the molecules that follow. Equilibrium MD is usually used to compute transport diffusivity efficiently and has

Table IV : A comparison of diffusion coefficients (the units are cm^2/s) for CH_4 molecules in equilibrium and averaged over all molecules (those in equilibrium and those not in equilibrium) over 150 ps at a density of 0.147 g/cm^3.

Nanotube type	0.147g/cm^3	
	Average	Equilibrium
(10,0)	3.25 x10^{-4}	3.23 x10^{-4}
(8,8)	1.44 x10^{-4}	1.41 x10^{-4}
(10,10)	7.70 x10^{-4}	7.64 x10^{-4}
(12,12)	2.45 x10^{-5}	2.38 x10^{-4}

shown good agreement with experimental data in zeolites [Sholl, Lee (2000)]. We have therefore reanalyzed the simulation results and examined the diffusion of only the molecules in equilibrium with each other and their surroundings and for which the environment, including molecular density, is identical. As the molecular density increases, the time needed to achieve equilibrium varies from 4 to 20 ps. The equilibrium diffusion coefficients for CH_4 at various densities and diffusing in various nanotubes are shown in Table IV and are compared with the average (equilibrium and non-equilibrium) diffusion coefficients for CH_4 in the same nanotubes. The results show that the equilibrium diffusion coefficients are almost the same as the average values at the lower molecular density of 0.147 g/cm^3. At higher molecular densities of 0.268 g/cm^3 (not shown in the table), the equilibrium values are about slightly lower than the average value.

A comparison is made between the binary Onsager diffusion coefficient for a CH_4/n-C_4H_{10} mixture from Eq. 6 and the diffusion coefficient of CH_4 from Eq. 2. The results are shown in Table V for diffusion in a (8,8) nanotube. The comparison shows that the two results are similar, although A increases slightly and D decreases as molecular density increases. The reason for these trends is that the loading of molecules inside the nanotubes changes with the molecular density. As the molecular density changes in small diameter nanotubes, the loading of the n-C_4H_{10} molecules goes up which hampers the motion of the CH_4 molecules. This causes the degree of molecular separation to decrease despite the fact that the loading of the CH_4 is also increasing. The interference in the diffusion of the CH_4 from the increased presence of n-C_4H_{10} cancels the density-gradient driving force on the molecules in nanotubes with smaller diameters. Therefore the diffusion coefficient of CH_4 changes little with changes in molecular density in (8,8) nanotubes. As the size of nanotubes increases, the density-gradient driving force becomes stronger and the diffusion coefficients of both CH_4 and n-C_4H_{10} increase. It should be pointed out here that the difference between A and D is due to the fact that the Onsager diffusion coefficient corresponds to the equilibrium diffusion state in the nanotubes while A is the average value for molecules in non-equilibrium and equilibrium conditions.

Table V : A comparison of diffusion coefficients A from Eq. 3 and D from Eq. 8 of CH_4 in a CH_4/n-C_4H_{10} mixture under different initial molecular densities in (8,8) nanotubes.

Initial Density (g/cm^3)	0.147	0.268
D (cm^2/s)	12.15 x10^{-5}	12.83 x10^{-5}
A (cm^2/s)	14.12 x10^{-5}	13.85 x10^{-5}

4 Conclusions

Classical MD simulations have been used to quantify the mass transport of organic and inorganic molecules and molecular mixtures by diffusive motion through carbon nanotubes and nanotube bundles. In all cases the diffusion occurred through the interior of the opened and C-atom terminated or H-atom terminated carbon nanotubes. Nanotubes of various helical symmetries are considered. Depending on the molecular size and shape and the nanotube diameter, in some cases molecules follow a spiral diffusive path to maximize their bond overlap with the C-C bonds in the carbon nanotube walls. In other cases, the molecules traveled down the center of the nanotube or absorbed to the nanotube walls. No diffusive in channels between nanotubes is observed, although it is expected that such diffusion would occur in channels larger than those considered here.

Acknowledgement: This work was supported by the NASA Ames Research Center and the Advanced Carbon Materials Center at the University of Kentucky, which is funded by the National Science Foundation through grant number DMR-9809686. The authors thank D. Sholl, P. Keblinski, E. Grulke, M. Jagtoyen, Rodney Andrews, and F. Derbyshire for many helpful discussions.

References

Allen, M. P.; Tildesley, D. J. (1987): *Computer Simulation of Liquids* (Oxford University Press, New York).

Ayappa, F. (1999): Journal of Chemical Physics **111**, 9082.

Ayappa, J.; Grulke, E. A.; Sinnott, S. B.; Qian, D.; Andrews, R.; Jagtoyen, M. (2001): Langmuir **17**, 7540.

Ayappa, K. G. (1998): Langmuir **14**, 880.

Benes, N.; Verweij, H. (1999): Langmuir **15**, 8292.

Bienfait, M.; Asmussen, B.; Johnson, M.; Zeppenfeld, P. (2000): Surface Science **460**, 243.

Bird, R.; Stewart, W.; Lightfoot, E. (1976): *Transport Phenomena* (John Wiley & Sons, New York).

Brenner, D. W. (1990): Phys. Rev. B **42**, 9458.

Brenner, D. W.; Shenderova, O. A.; Harrison, J. A.; Stewart, S. J.; Ni, B.; Sinnott, S. B. (in press): J. Phys. C: Condens. Matter.

Breton, J.; Gonzalez-Platas, J.; Girardet, C. (1994): Journal of Chemical Physics **101**, 3334.

Brown, C. M.; Yildirim, T.; Neumann, D. A.; Heben, M. J.; Gennett, T.; Dillon, A. C.; Alleman, J. L.; Fischer, J. E. (2000): Chemical Physics Letters **329**, 311.

Caruana, C. M. (1997): Chem. Eng. Progress **March**, 17.

Chen, P.; Wu, X.; Lin, J.; Tan, K. L. (1999): Science **285**, 91.

Cheryan, M. (1986): *Ultrafiltration Membranes* (Technomic Publishing Company, Inc., Pennsylvania).

Cole, M. W.; Crespi, V. H.; Stan, G.; Ebner, C.; Hartman, J. M.; Moroni, S.; Boninsegni, M. (2000): Physical Review Letters **84**, 3883.

Cui, S. T.; Cochran, H. D.; Cummings, P. T. (1999): J. Phys. Chem. B **103**, 4485.

Cuthbert, T. R.; Wagner, N. J.; Paulaitis, M. E.; Murgia, G.; D'Aguanno, B. (1999): Macromolecules **32**, 5017.

Darkrim, F.; Levesque, D. (1998): Journal of Chemical Physics **109**, 4981.

Darkrim, F.; Levesque, D. (2000): Journal of Physical Chemistry B **104**, 6773.

Dillon, A. C.; Jones, K. M.; Bekkedahl, T. A.; Kiang, C. H.; Bethune, D. S.; Heben, M. J. (1997): Nature **386**, 377.

Dillon, A. C.; Jones, K. M.; Bekkedahl, T. A.; Kiang, C. K.; D. S. Bethune; Heben, M. J. (1997): Nature **386**, 377.

Dresselhaus, M. S.; Williams, K. A.; Eklund, P. C. (1999): MRS Bulletin **24**, 45.

Ebbesen, T. W. (1996): J. Phys. Chem. Solids **57**, 951.

Eswaramoorthy, M.; Sen, R.; Rao, C. N. R. (1999); Chem. Phys. Lett. **304**, 207.

Fan, X.; Dickey, E. C.; Eklund, P. C.; Williams, K. A.; Grigorian, L.; Buczko, R.; Pantelides, S. T.; Pennycook, S. J. (2000): Physical Review Letters **84**, 4621.

Garg, A.; Han, J.; Sinnott, S. B. (1998): Physical Review Letters **81**, 2260.

Gear, C. W. (1966): Numerical Integration of Ordinary Differential Equations of Various Orders, Argonne National Laboratory.

Gear, C. W. (1971): *Numerical Initial Value Problems in Ordinary Differential Equations* (Prentice-Hall, Englewood Cliffs, New Jersey).

Gergidis, L.; Theodorou, D.; Jobic, H. (2000): J. Phys. Chem. B **104**,5541.

Gladden, L. F.; Sousa-Goncalves, J. A.; Alexander, P. (1997): J. Phys. Chem. B **101**, 10121.

Gordon, P. A.; Saeger, R. B. (1999): Ind. Eng. Chem. Res. **38**, 4647.

Hahn, K.; Karger, J. (1998): J. Phys. Chem. B **102**, 5766.

Iijima, S. (1991): Nature **56**, 354.

Iijima, S.; Brabec, C.; Maiti, A.; Bernholc, J. (1996): Journal of Chemical Physics **104**, 2089.

Karger, J.; Ruthven, D. M. (1992): *Diffusion in Zeolites and Microporous Solids* (Wiley and Sons, New York).

Keffer, D.; Davis, H. T.; McCormick, A. V. (1996): Adsorption **2**, 9.

Keffer, D.; McCormick, A. V.; Davis, H. T. (1996): Mol. Phys. **87**, 367.

Keffer, D. (1999): Chem. Eng. J. **74**, 33.

Kuznetsova, A.; Mawhinney, D. B.; Naumenko, V.; John, J.; Yates, T.; Liu, J.; Smalley, R. E. (2000): Chemical Physics Letters **321**, 292.

Lee, S. M.; Lee, Y. H. (2000): Applied Physics Letters **76**, 2877.

Liu, J. (1998): , *et al.*, Science **280**, 1253

Liu, C.; Fan, Y. Y.; Liu, M.; Cong, H. T.; Cheng, H. M.; Dresselhaus, M. S. (1999):Science **286**, 1127.

MacElroy, J.; Boyle, M. (1999): Chem. Eng. J. **74**, 85.

Mao, Z.; Garg, A.; Sinnott, S. B. (1999): Nanotechnology **10**, 273.

Mao, Z.; Sinnott, S. B. (2000) J. Phys. Chem. B **104**, 4618.

Mao, Z.; Sinnott, S. B. (2001): J. Phys. Chem. B, 6916.

Morooka, S.; Kusakabe, K. (1999): MRS Bull, 25.

Mosell, T.; Schrimpf, G.; Brichmann, J. (1997): J. Phys. Chem. B **101**, 9476.

Mosell, T.; Schrimpf, G.; Brichmann, J. (1997): J. Phys. Chem. B **101**, 9485.

Muris, M.; Dufau, N.; Bienfait, M.; Dupont-Pavlovsky, N.; Grillet, Y.; Palmari, J. P. (2000): Langmuir **16**, 7019.

Murthy, C. S.; O'Shea, S. F.; McDonald, I. R. (1983): Mol. Phys. **50**, 531.

Nelson, P. H.; Scott, M. A. (1999): J. Chem. Phys. **100**, 9235.

Nutzenadel C.; Zuttel, A.; Chartouni, D.; Schlapbach, L. (1999): Electrochem. Solid-State Lett. **2**, 30.

Pederson, M. R.; Broughton, J. Q. (1992): Phys. Rev. Lett. **69**, 2689.

Ryckaert, J.P.; Bellemans, A. (1975): Chem. Phys. Lett. **30**, 123.

Rzepka, M.; Lamp, P.; Casa-Lillo, M. A. d. l. (1998): Journal of Physical Chemistry B **102**, 10894.

Sanborn, M.; Snurr, R. (2000): **20**, 1.

Saravanan, C.; Auerbach, S. M. (1999): J. Chem. Phys. **110**, 11000.

Sastre, G.; Catlow, C. R. A.; Corma, A. (1999): J. Phys. Chem. B **103**, 5187.

Sholl, D. S.; Fichthorn, K. A. (1997): J. Chem. Phys. **107**, 4384.

Sholl, D. S. (1999): Chem. Eng. J. **74**, 25.

Sholl, D.; Lee, C. (2000): J. Chem. Phys. **112**, 817.

Simonyan, V. V.; Diep, P.; Johnson, J. K. (1999): Journal of Chemical Physics **111**, 9778.

Sinnott, S. B.; Andrews, R. (2001): Crit. Rev. Solid State Mater. Sci. **26**, 145.

Sloan, J.; Hammer, J.; Zwiefka-Sibley, M.; Green, M. L. H. (1998): Chem. Commun. **3**, 347.

Stan, G.; Cole, M. W. (1998): Surface Science **395**, 280.

Teizer, W.; Hallock, R. B.; E. Dujardin; Ebbesen, T. W. (1999): Physical Review Letters **82**, 5305.

Teizer, W.; Hallock, R. B.; Dujardin, E.; Ebbesen, T. W. (2000): Physical Review Letters **84**, 1844.

Ugarte, D.; Chatelain, A.; de Heer, W. A. (1996): Science **274**, 1897.

Vidales, A. M.; Crespi, V. H.; Cole, M. W. (1998): Physical Review B **58**, R13426.

Wang, Q.; Johnson, J. K. (1999): Journal of Physical Chemistry B **103**, 4809.

Wang, Q.; Johnson, J. K. (1999): Journal of Chemical Physics **110**, 577.

Webb III, E. B.; Grest, G. S.; Mondello, M. (1999): J. Phys. Chem. B **103**, 4949.

Weber, S. E.; Talapatra, S.; Journet, C.; Zambano, A.; Migone, A. D. (2000): Physical Review B **61**, 13150.

Yakobson, B. I.; Brabec, C. J.; Bernholc, J. (1996): Physical Review Letters **76**, 2511.

Yang, Y. T. (2000): Carbon **38**, 623.

Ye, Y.; Ahn, C. C.; Witham, C.; Fultz, B.; Liu, J.; Rinzler, A. G.; Colbert, D.; Smith, K. A.; Smalley, R. E. (1999): Applied Physics Letters **74**, 2307.

Yin, Y. F.; Mays, T.; McEnaney, B. (2000); Langmuir **16**, 10521.